Quantitative Analysis of Superparamagnetic Contrast Agent in Sentinel Lymph Nodes Using *Ex Vivo* Vibrating Sample Magnetometry

Martijn Visscher*, Joost J. Pouw, Joop van Baarlen, Joost M. Klaase, and Bennie ten Haken

***Abstract*—As the first step in developing a new clinical technique for the magnetic detection of colorectal sentinel lymph nodes (SLNs), a method is developed to measure the magnetic content in intact, formalin fixated lymph nodes using a vibrating sample magnetometer (VSM). A suspension of superparamagnetic nanoparticles is injected *ex vivo* around the tumor in the resected colon segments. A selection of three lymph nodes is excised from the region around the tumor and is separately measured in the VSM. The iron content in the lymph nodes is quantified from the magnetic moment curve using the Langevin model for superparamagnetism and a bimodal particle size distribution. Adverse, parasitic movements of the sample were successfully reduced by tight fixation of the soft tissue and using a small vibration amplitude. Iron content in the lymph nodes is detected with 0.5 μg accuracy and ranged from 1 to 51 μg. Histological staining confirmed iron presence. The current method of measuring intact biological tissue in a VSM is suitable to show the feasibility and merit of magnetic detection of SLNs in colorectal cancer. For clinical validation of magnetic SLN selection in colorectal cancer, a new magnetometer with high specificity for superparamagnetic nanoparticles is required.**

***Index Terms*—Biological samples, magnetic detection, sentinel lymph node (SLN), vibrating sample magnetometry (VSM).**

I. Introduction

MAGNETIC nanoparticles have become increasingly important in both noninvasive and minimally invasive medical applications [1], [2]. Superparamagnetic nanoparticles have already been used as contrast agents in magnetic resonance imaging (MRI) for a long time [3], [4]. Furthermore, the use of magnetic nanoparticles for drug delivery [5]–[8] and hyperthermia treatment [9] remains under development. One of the new developments is the use of magnetic nanoparticles for sentinel lymph node (SLN) detection. In Japan and the U.K., magnetic detection of SLNs using a handheld probe was developed for lung [10], [11] and breast cancer [12]–[14]. Similar experiments using a high-T_C SQUID gradiometer were demonstrated in a rat model [15]. A recent study shows the applicability of magnetic nanoparticles as contrast agent for photoacoustic imaging which can provide intraoperative lymph node staging [16]. The present clinical procedure of SLN detection includes selection of the lymph nodes that drain the tumor area by a technetium marker and blue dye to apply advanced microscopic analysis (ultrastaging) to detect metastasis [17], [18]. The presence of metastasis is important for disease staging and subsequent clinical decisions. SLN biopsy helps the pathologist to select nodes with the highest chance for (micro)metastasis. When no metastasis is found with normal hematoxylin and eosin (H and E) staining, ultrastaging—which is time consuming—can be exclusively restricted to the SLNs.

The introduction of magnetic nanoparticles in SLN procedures can improve diagnosis and therapy for various tumors. In case of colorectal cancer, diagnosis can be improved by more specific selection of the SLNs. This can increase staging accuracy and subsequently, it can help to plan an adequate therapeutic path [19]. In breast cancer and melanoma, magnetic SLN detection has to compete with the well performing, but logistically more complex, combined method using radioactive tracer and blue dye. Magnetic detection largely simplifies logistics and safety protocols and makes potentially accurate SLN detection accessible for hospitals that do not have a department for nuclear medicine. In those hospitals significant therapeutic improvements can be achieved by introduction of a reliable SLN procedure.

In surgical procedures of colorectal cancer, a complete colon segment is resected including all lymph nodes surrounding the tumor. Sentinel lymph node mapping (SLNM) for this type of cancer is still in development and is potentially highly beneficial [20]–[25]. The procedure is introduced to obtain a more precise diagnosis and is technically still developing regarding tracers and surgical approach. The majority of studies use only a blue dye as contrast agent and are performed either *in vivo* or *ex vivo* [19]. A suspension of superparamagnetic iron oxide (SPIO) nanoparticles is an attractive alternative for both blue dye and technetium in colorectal cancer.

The added value of magnetic nanoparticles compared to the generally used technetium and blue dye tracers is that they are stable and, therefore, detectable and quantifiable over time. The

Manuscript received October 22, 2012; revised March 27, 2013; accepted April 22, 2013. Date of publication May 6, 2013; date of current version August 16, 2013. *Asterisk indicates corresponding author.*

*M. Visscher is with the Neuro-Imaging Group, MIRA Institute for Biomedical Engineering and Technical Medicine, University of Twente, 7500 AE Enschede, The Netherlands (e-mail: m.visscher@utwente.nl).

J. J. Pouw and B. ten Haken are with the Neuro-Imaging Group, MIRA Institute for Biomedical Engineering and Technical Medicine, University of Twente, 7500 AE Enschede, The Netherlands (e-mail: j.j.pouw@utwente.nl; b.tenhaken@utwente.nl).

J. van Baarlen is with the Laboratorium Pathologie Oost-Nederland and Medisch Spectrum Twente, 7500 AE Enschede, The Netherlands (e-mail: j.vanbaarlen@laborpath.nl).

J. M. Klaase is with the Department of Surgery, Medisch Spectrum Twente, 7500 AE Enschede, The Netherlands (e-mail: J.Klaase@mst.nl).

Color versions of one or more of the figures in this paper are available online at http://ieeexplore.ieee.org.

Digital Object Identifier 10.1109/TBME.2013.2261893

restricted lifetime of technetium-99m and the fluidity of blue dye limit the time frame of reliable detection of the SLN after surgery. The use of a physically more stable tracer allows *ex vivo* detection several hours after surgery. In such an *ex vivo* procedure, the SLN detection aims to make an accurate selection out of all harvested lymph nodes, rather than a search in a tissue mass for one specific tracer containing lymph node. All lymph nodes are individually selected as SLN based on the presence of magnetic tracer. This postoperative procedure reduces the burden on costly operating time.

Another advantage of a tracer with particles is to reduce the chance to select higher echelon nodes. The particles in a magnetic tracer are more easily trapped in the SLN compared to the fluidic blue dye that may spread further to higher echelon nodes [26]. At present, it is still unknown whether these nanoparticles will end up in the SLNs (first echelon) after *ex vivo* injection. Physiological processes in the lymphatic system, like macrophage activity, are expected to stop soon after resection. Moreover, detection of *ex vivo* particle uptake can be limited because the lymph nodes in the mesenterium are rather small in size and *ex vivo* infiltration of particles might be low. The experiments in this first study have to show whether the nanoparticles can still accumulate in the SLNs in *ex vivo* circumstances.

The stability of a magnetic tracer provides the opportunity for a feasibility study of *ex vivo* magnetic SLN detection in colorectal cancer in an extramural laboratory. Therefore, a clinically suitable instrument is not needed *a priori*. Detection of SPIO in an SLNM procedure serves to decide whether a particular lymph node is a candidate for additional microscopic analysis. The detection system has to give a decisive answer about the presence of tracer. Therefore, a highly sensitive and specific detection system is required. Spatial imaging of tracer is inferior to a more reliable indicator of tracer presence. Therefore, magnetometry methods selectively sensitive for nonlinear magnetic properties of SPIO are preferred over less specific laborious quantitative MRI techniques that are susceptible to assumptions about background signals from tissue, (geometry of) SPIO distribution and detection thresholds [27]. Different spectroscopic methods that have been developed to quantify SPIO content in cell samples, require sample digestion and are, therefore, not compatible with histopathologic analysis in a SLNM procedure [28]. In this study, the SLNs were quantitatively analyzed using a standard vibrating sample magnetometer (VSM). Quantification of particle uptake serves to determine technical requirements for development of a clinically suitable magnetometer.

The magnetic analysis of fresh or formalin-fixated biological tissue using a VSM is a challenging procedure. In several studies, magnetometry of biological tissue was achieved at rather low temperatures ($T < 273$ K) or after freeze-drying the sample to enable a firm fixation [29]–[34]. Such a procedure is problematic if the sample has to remain intact for clinical histological analysis. Therefore, in the present study a reliable, nondestructive VSM-method was developed to measure the magnetic content of SPIO particles in intact diamagnetic biological samples at room temperature. Despite the time-consuming and clinically impractical technique of VSM, the measurements provide important information for the development of a clinical magnetometer to replace the VSM in the methodology presented here.

The objective of the current study is first to show, with a limited number of experiments, the feasibility of magnetic nanoparticles as tracer for *ex vivo* SLNM in colorectal cancer. The second objective is to determine the quantitative requirements for a clinically suitable magnetometer that can perform fast *ex vivo* analysis of the colorectal lymph nodes. Since the focus in this study is on the technical feasibility of magnetic nanoparticles in *ex vivo* colorectal tissue, the patient-specific clinical results and their consequences are topic of future papers.

II. Experiments

A. Superparamagnetic Particles and Clinical Application

The Endorem MRI contrast agent (Guerbet Nederland B.V., Gorinchem, The Netherlands) is chosen as superparamagnetic tracer for identification of the SLNs. This tracer is a suspension of SPIO nanoparticles coated with dextran in a concentration of 11.2 mg iron per mL. The hydrodynamic particle size is reported in a range of 58–186 nm [35], [36]. The lymph nodes are harvested from resected tissue of patients with colorectal cancer who underwent a standard surgical procedure. Immediately after resection, the colon part containing the tumor is brought to a separate field and is injected submucosally around the tumor with 1.5–2.0 mL of Endorem and massaged for about 5 min to induce particle flow into the lymphatic system. Macrophage activity responsible for *in vivo* lymphatic processing of magnetic nanoparticles [37] is expected to stop immediately after resection. Therefore, mechanical transport of particles through the interstitial space and the lymphatics should be maintained *ex vivo* to get the SLNs filled with tracer. Since VSM analysis of all the lymph nodes in each specimen would be very time consuming and magnetic detection of the lymph nodes *in situ* was not possible, a parallel SLN selection procedure with blue dye is used. Patent Blue V (Guerbet Nederland B.V., Gorinchem, The Netherlands) is injected additionally after Endorem to enable the visual selection of SLNs by the pathologist. For each patient, the blue lymph nodes nearest to the tumor, with a maximum of three, are considered as SLNs and are resected for analysis of iron content and placed in formalin for 24–72 h. The local ethics committee of the hospital Medisch Spectrum Twente in Enschede was informed and agreed with the experimental procedure.

B. Sample Placement

All samples are placed in an NMR glass tube (Wilmad-LabGlass, Vineland, NJ, USA) with an inner diameter of 8.16 mm and an outer diameter of 10 mm. To prevent uncontrolled movement during VSM-measurements, the samples are fixated between two plastic parts inside the tube [see Fig. 1(a)]. The upper part is adjustable in length to allow for different sample sizes; typically for lymph nodes between 2 and 10 mm. In addition, the soft lymphatic tissue with some surrounding fat can

Fig. 1. (a) Lymph node sample fixated with plastic system in glass tube. (b) VSM detection coil set with bore diameter 10.6 mm.

be compactly fixated. To reduce noise from liquid movement, the level of remnant formalin in the tube is as low as possible. Automatic offset detection by the VSM system itself is often not accurate because of low or absent magnetization in biological tissue. Therefore, the axial distance from the bottom of the tube to the center of the sample is measured manually to determine the optimal VSM-offset position in the detection coil set.

C. VSM Procedure

Measurements are performed using the VSM of a physical property measurement system (PPMS, Quantum Design Inc., San Diego, CA, USA) with a maximum magnetic field capacity of $\mu_0 H = 9$ T. The applied field range is lower ($\mu_0 H = 4$ T) to prevent samples from large forces while approaching magnetic saturation for Endorem particles. The vibration frequency was 40 Hz, whereas the vibration amplitude was 0.5 mm. This low amplitude reduces the forces acting on the sample by a factor of 4, compared to the default amplitude of 2 mm. Consequently, noise caused by interfering, parasitic movements due to soft tissue is reduced. The lymph nodes are relatively large compared to most samples normally measured in a VSM. To fit the NMR tube containing the lymph node, a custom-made VSM detection coil was used with an inner diameter of 10.6 mm [see Fig. 1(b)].

To investigate sensitivity of magnetic detection and to calibrate the VSM for Endorem containing lymph nodes, a series of calibration samples was prepared. Small glass containers were filled with 15 μL diluted Endorem ranging from 1:1 to 1:150, which corresponds with 168 to 1.12 μg iron in a sample. In addition, some larger samples containing 500 and 1568 μg iron were used to increase accuracy of the calibration factor. Furthermore, a known Endorem sample is measured while immersed in formalin to investigate the noise contributions from free liquid formalin. Samples with Patent Blue V and formalin are measured to exclude the effect of superparamagnetic or ferromagnetic contributions when present in lymph node samples. To determine the correction for the demagnetization of the superconducting magnet [38], a paramagnetic palladium sample is measured in the same field range as applied to the lymph nodes.

D. Data Analysis

VSM measurements of lymph nodes placed in the NMR tube with plastic fixation parts are assumed to exhibit a superparamagnetic component originating from the nanoparticles, a diamagnetic component originating from the tissue and a paramagnetic component originating from the sample holder. Magnetic moment versus field curves of the sample were analyzed in MATLAB (The Mathworks Inc., Natick, MA, USA) by a parameter optimization of a model that includes the three different magnetic components. Before the optimization, some preprocessing of the data was necessary to remove some additional effects from the data, which is explained hereafter.

In the first step, a correction is made to the measured field to compensate for demagnetization of the superconducting magnet in the PPMS [38]. The palladium measurement should theoretically show a strictly anhysteretic linear curve. Any hysteresis observed in this measurement can be attributed to the demagnetization of the magnet during the measurement. This causes an inaccurate field measurement that should be corrected to obtain coinciding ascending and descending branches in measurements of anhysteretic materials. To compensate for demagnetization of the superconducting magnet, a field correction of 1750 A/m is applied to each dataset. Then, the assumption is made that no hysteresis is present in the Endorem sample at ambient temperatures [39] and the Langevin model for superparamagnetism can be applied.

The strength of the linear components in the measurements vary over different samples and are eliminated from the optimization by subtracting the linear approximation of the magnetic moment in the high field region. In most studies, this component is determined by a "background" measurement. There are three reasons why this cannot be done in the current study: 1) the magnetic contribution from tissue cannot be determined in a separate measurement before tracer administration and depends on the size of a lymph node and the amount of surrounding fat and thus, differs for each lymph node, 2) the amount of formalin surrounding the sample varies, and 3) since the variable size of the calibration samples and lymph nodes needs fine-tuning of the fixation system, the paramagnetic contribution of the sample holder in the detection coil differs from sample to sample. Therefore, the sample-dependent linear component is approximated by a linear fit of the data measured from 90% of the field maxima ($|H|_{\max}$). The superparamagnetic component of the magnetic moment of the sample is assumed to be saturated in this region. Although this is not true for contributions of very small superparamagnetic particles, this approach can be used when the model describing the superparamagnetic component is subjected to the same procedure. Therefore, the model is also subjected to a linear subtraction, which is based on the slope of the modeled superparamagnetic component in the same high field range as the measured data. So, to obtain the most likely parameters describing the curvature of the magnetic moment curve, the model and the data are matched in the

high field region by linear approximation, while the particle size distribution parameters in the fitting algorithm that describe the unsaturated nonlinear superparamagnetic part are optimized by minimization of the error between data and fit.

Asymmetry in the positive and negative branches of the measured curve was treated by an offset correction. Finally, the magnetic moment curve is normalized in order to exclude the saturation value from the parameters to be optimized. Then, a normalized model for the superparamagnetic component can be compared with the normalized data.

The optimization procedure is now only dependent on the *shape* of the superparamagnetic components, which is determined by the particle characteristics in the sample. The superparamagnetic component is modeled by the Langevin model for superparamagnetism [40], described by

$$L(x_k H) = \coth(x_k H) - \frac{1}{x_k H} \tag{1}$$

with

$$x_k H = \frac{m_k \mu_0 H}{k_B T}. \tag{2}$$

The constants μ_0, k_B and parameter T represent vacuum permeability, the Boltzmann constant, and the absolute temperature (always 300 K in our case), respectively. The Langevin function is specific for a particle size with magnetic moment m_k [A·m^2] and depends on the applied magnetic field strength H [A/m]. Since the size of a magnetic nanoparticle determines its magnetic moment, a sample with a certain particle size distribution has also a certain magnetic moment distribution. Therefore, the model describing the experimental data has to take into account a distribution of magnetic moments [41]. The magnetic moment of a superparamagnetic particle is related to its diameter D_k [m] by the bulk saturation magnetization M_s [A/m] of iron oxide Fe_3O_4 ($\mu_0 M_s = 0.60$ T, [41]) via

$$m_k = \frac{\pi D_k^3 M_s}{6}. \tag{3}$$

For magnetic nanoparticles, a unimodal log-normal particle size distribution is generally accepted [42], because it is physically very likely and can be explained by physical phenomena during the production process [43]. Furthermore, transmission electron microscopy results of Endorem indicated a log-normal core size distribution [39]. The numerical approach of the log-normal particle size distribution is defined as

$$f(D_k|D_1,\sigma_1) = \frac{1}{D_k \sigma_1 \sqrt{2\pi}} e^{\frac{-\ln(D_k - D_1)}{2\sigma_1^2}}, \quad k = (1,\ldots,K) \tag{4}$$

where D_1 and σ_1 are the mean diameter and standard deviation of the associated normal distribution, respectively. The distribution is calculated for a broad range of K different particle diameters with diameter step size D_{step}. By substituting (3) for each D_k into (1) and (2) and multiplying each resulting Langevin function by its weight from the distribution $f(D_k|D_1,\sigma_1)\cdot D_{\text{step}}$, the contribution from each particle size is computed.

However, the model of the magnetic moment curve using a unimodal log-normal distribution for Endorem did not result in a suitable approach of the data. Especially in the region of the strongest curvature, the model cannot match the data. Therefore, the unimodal log-normal distribution cannot represent the core size distribution of Endorem and a core size distribution with other shape parameters has to be used. Since particle production processes often result in log-normal distributed populations, it is reasonable to add a second log-normal distribution in the fit, which gives more degrees of freedom to the modeling curve. The bimodality of the particle size distributions may originate from the production process of the nanoparticles. A chemical growth process, such as precipitation used for Endorem production [39], [44], comprises initial nucleation and growth, after which some original (smaller) seeds may remain in the colloid, which gives rise to two log-normal distributed particle size populations [45]. In present analysis, the bimodal distribution is only a way to model the most probable experimental magnetic moment curve using the most relevant parameters of the size distribution. Implementation of a bimodal log-normal distribution requires three additional parameters to be optimized: a second mean and standard deviation for the distribution and the relative weight factors p and $(1-p)$ for each distribution.

Finally, the sum of all modeled Langevin functions for the bimodal log-normal distribution describes the model to be optimized

$$m(H) = \sum_{k=1}^{K} n \frac{\pi D_k^3 M_s}{6} \cdot L(x_k H) \cdot f(D_k|D_1,D_2,\sigma_1,\sigma_2,p) \cdot D_{\text{step}}, \quad (k = 1,\ldots,K) \tag{5}$$

where m represents the total field-dependent magnetic moment of the sample and n the number of particles. This model as well as the data is normalized and the best parameters are determined by minimization of the root of the sum of squares of the logarithmic differences between the model $m(H)$ and measurement data $m_{\text{sample}}(H)$ [46]:

$$Error = \sqrt{\sum_{H=H_{\min}}^{H_{\max}} \left(\log|m(H)| - \log|m_{\text{sample}}(H)|\right)^2}. \tag{6}$$

This minimization for five parameters is performed using the Nelder–Mead simplex algorithm, which is an unconstrained nonlinear optimization algorithm implemented in the MATLAB software package [47]. The minimization gives optimal parameters for the particle size distribution.

After the optimum distribution has been determined, the original superparamagnetic component, which is lost in the normalization, can be reconstructed. The linear subtraction applied to the model is added again to both the normalized model and the normalized measured data. The total magnetic moment responsible for superparamagnetism in a sample is determined by the sum of magnetic moments of the individual particles. This can be derived from the factor that was used for normalization of the data. To finish the quantitative reconstruction of the

superparamagnetic component, both model and data were multiplied by this factor, which is basically the saturated magnetic moment.

For relatively large linear contributions in lymph node measurements, the quantification of the superparamagnetic component is very sensitive for noise, since after linear correction the relatively small errors made at high fields have a large effect on the small amplitude of the superparamagnetic component. Therefore, reduction of movement noise is particularly important for the quantification of samples with low amounts of iron. Determination of all parameters of the bimodal particle size distribution is, therefore, not suitable for each individual lymph node measurement. For that reason, the parameters of the particle size distributions found for the calibration samples are averaged and used in the model to quantify the iron content in lymph nodes. This average bimodal distribution is based on all measurements of calibration samples with an fit error lower than 0.5 [see (6)]. Thereby, it is assumed that the particle size distribution of the superparamagnetic cores in the lymph nodes is the same as in the original tracer. The hydrodynamic size distribution of the particles that enter the lymph nodes might be different from the distribution in the original tracer, because the tissue and lymphatic system can be considered as a filter that may trap the larger particles. In the lymph node analysis presented here, the core size distribution in lymph nodes is assumed to be the same as in the original tracer, which supposes that hydrodynamic size is not directly related to magnetic core size. Finally, there remain three parameters to be estimated for the lymph node measurement. The first parameter is the saturated magnetic moment m_s, which corresponds to the amount of iron. The second parameter is the linear component χH, added to estimate the volumetric susceptibility χ of paramagnetic or diamagnetic material. The last estimate is an offset correction that is applied to correct for asymmetry.

E. Light Microscopic Analysis of Lymph Nodes

Following VSM measurements, the lymph nodes are sliced (2–4 μm) for histological analysis by a pathologist. The presence of metastases is revealed by H and E and Cam 5.2 histological staining. Pearls Prussian Blue staining is used to indicate iron content in the lymph nodes.

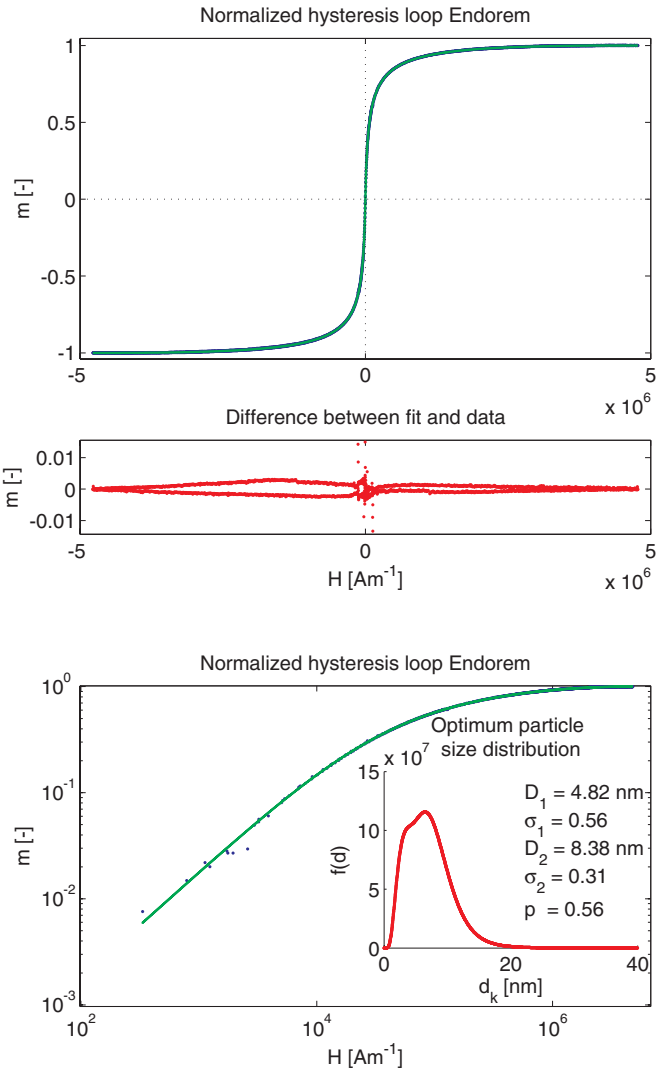

Fig. 2. Normalized magnetic moment versus field curve. The *upper panel* shows the normalized measurement and the curve of the optimized model on linear scale. The *mid panel* shows the difference between the model and the measured data. The negative and positive differences indicate that the model is well positioned in between the descending and ascending branch of the loop, showing some unphysical hysteresis due to measurement error. The *lower panel* on bilogarithmic scale gives more insight in the quality of measured data and the model in the low field region. Superparamagnetism is confirmed by the absence of significant hysteresis in the low field region. The bimodal log-normal particle size distribution that resulted in the best modeling curve is shown in the *inset*.

III. Results and Discussion

A. Calibration and Parameter Modeling

Different samples with a known quantity of Endorem were used as reference measurement to calibrate the system, as well as to develop the parameter modeling of the total magnetic moment of a sample. The model achieved for the measured data and the accompanying bimodal particle size distribution is shown in Fig. 2. For the average particle size distribution further used for lymph node quantification, the following parameters were found: $D_1 = 4.5$ nm, $\sigma_1 = 0.47$, $D_2 = 8.3$ nm, $\sigma_1 = 0.29$, and $p = 0.52$. These values are in the same range as was found using a unimodal log-normal distribution for TEM analysis of Endorem nanoparticles [39], [48], [49]. The bimodal core size distribution has a more broadened peak compared to a unimodal log-normal distribution, but does not show two clear separate maximums. The use of the bimodal log-normal distribution does give more freedom to the shape of the distribution and does not implicate that there are two clearly distinguishable populations of particle sizes.

The deviation of the model from the measured data revealed a systematic measurement error (see Fig. 2). The ascending and descending branches of the loop do not coincide, which causes dissimilar differences between the measurement data and the model. This may indicate hysteresis in the sample, but the asymmetric and inconsistent pattern of deviation argues for measurement errors.

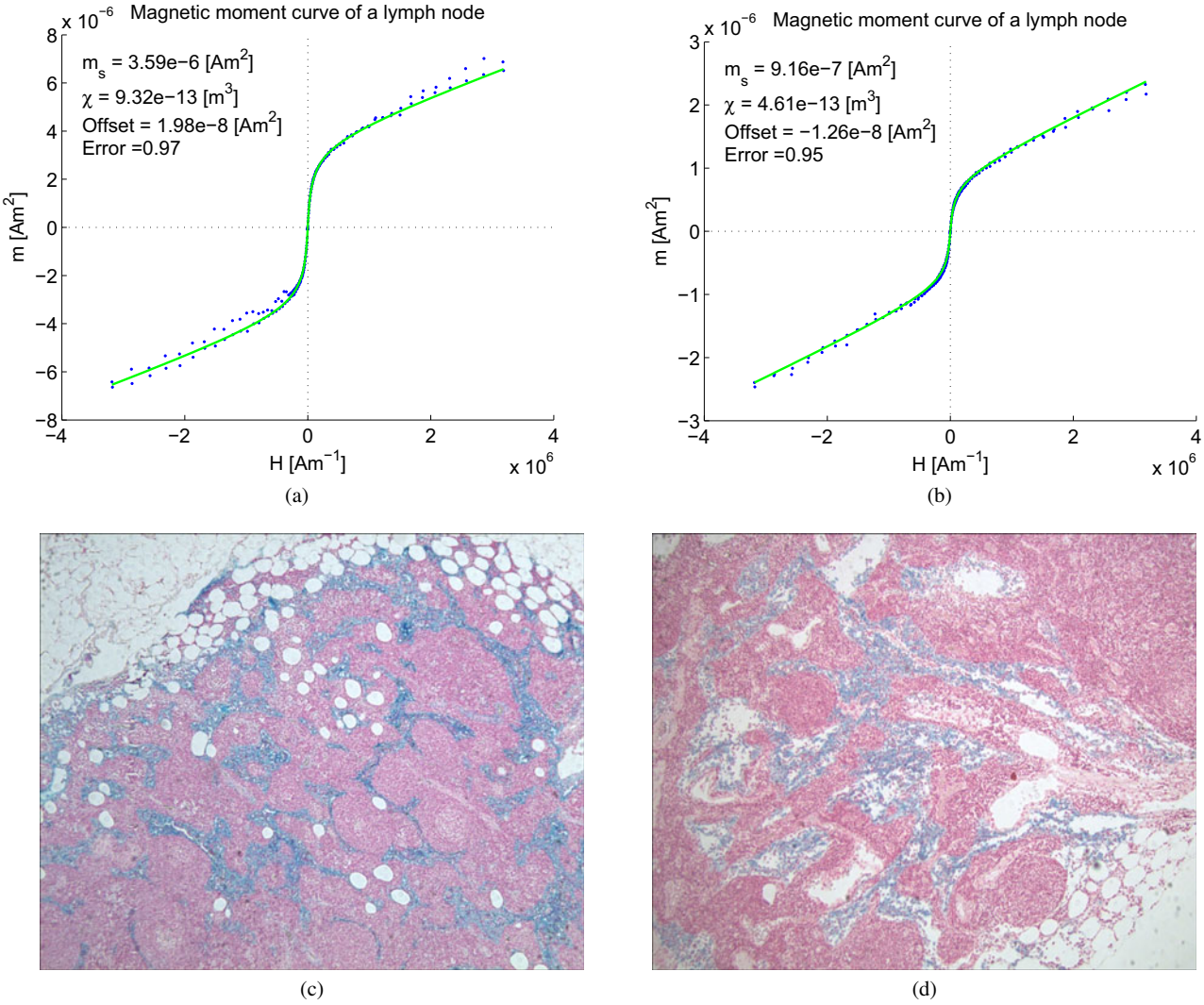

Fig. 3. Two examples of a VSM measurement of a lymph node containing Endorem and the corresponding microscopy images with Pearls Prussian Blue staining. Endorem content corresponds with (a) 46.7 μg and (b) 11.9 μg iron. The green line indicates the model applied to the data points measured, including a linear (χ) and nonlinear component with amplitude m_s. The corresponding histology images (c and d) with Pearls Prussian Blue confirm the presence of SPIO and indicate interstitial spread of the particles throughout the sinuses of the lymph nodes.

Since the saturated magnetization at a high field strength is used as calibration to estimate iron content in other samples, the model should be as precise as possible in this region. The calibration with the lowest amount of 1 μg iron could not accurately be quantified, but still shows a minor superparamagnetic component indicating the detection limit. The lowest amount of Endorem that could be quantified corresponds to 1.5 μg Fe with an error of ± 0.5 μg. This detection limit depends strongly on the quality of the measurement and the contribution of linear magnetic materials. The calibration constant used to quantify lymph node samples with a saturation field of $3.18 \cdot 10^6$ A/m was $7.76 \cdot 10^{-8}$ A·m^2 μg^{-1}.

Measurements of samples with Patent Blue V and formalin did not show any nonlinear magnetic contribution that may interfere with the superparamagnetic contribution from particles accumulated in the tissue (results not shown). So, the presence of Patent Blue V and formalin in or around lymph node samples will not affect an accurate estimation of the superparamagnetic component from the tracer.

B. Lymph Node Analysis

The magnetic content in lymph nodes is determined based on the average particle size distribution found in the calibration samples. The Endorem mass in the lymph nodes is determined using the Langevin model with the bimodal distribution described in Section II-D. Although in most cases a significant linear contribution was present, a superparamagnetic nonlinear component could be well estimated by the algorithm, and therefore, a background measurement became unnecessary. This is important, because a background measurement for the lymph nodes would even be impossible for this clinical application.

The magnetic moment curve of two lymph nodes is shown in Fig. 3. There is an obvious difference with the curve in Fig. 2

because of the linear contribution from sample holder and tissue. Both the superparamagnetic and the linear component are estimated by fitting the parameters m_s and χ, respectively. The calibration constant derived from a series of known Endorem samples (see Section. III-A) is used to determine the iron mass in the lymph node. Over all, from 13 patients and 33 lymph nodes included in the study, Endorem content was detected in 24 lymph nodes and was found in the range of 1.1–51.4 μg iron. The mean quantity of iron found in lymph nodes was 17.1 μg. Light microscopic analysis of the lymph nodes with Pearls Prussian Blue staining confirmed iron presence in each lymph node that was detected by magnetometry (see Fig. 3). The iron presence was observed in the interstitial space in all but one lymph node. In that particular lymph node macrophages stained positive for iron.

Some measurements suffered from significant noise and possibly sample displacement. The lymph node samples with a substantial proportion of fat tissue are more susceptible to abusive, parasitic, lateral movements. This is overcome by a stronger fixation of the sample, resulting in lower noise and subsequent accurate quantification of the amount of iron. The remaining effect of motion-generated errors is represented in the error of the fit procedure [see (6)], which is on average 1.61 for lymph nodes compared to 0.24 for the calibration samples. However, for the present study this error is small enough to obtain a quantitative indication of Endorem filling of colorectal lymph nodes in an *ex vivo* sentinel node procedure. Future systems for the magnetic lymph node analysis need to be designed such that this kind of errors do not occur.

There are two possible reasons that some blue nodes that were selected as SLNs by definition did not contain iron. First, the definition of the SLN may have failed by selecting lymph nodes that are not true SLNs. The probably more selective magnetic tracer has only reached the true SLNs in that case. This cannot be verified, since lymph node mapping is unable to reveal whether a lymph node is a first or higher echelon node. The second reason could be that the *ex vivo* circumstances reduced magnetic tracer migration toward lymph nodes. Therefore, some of the SLNs may be missed by the magnetic tracer. These aspects of the procedure should be investigated in a more elaborate clinical study that allows magnetic measurements on all the lymph nodes in a specimen.

Interestingly, the results show that *ex vivo* SLN mapping with magnetic nanoparticles is feasible. Lymphatic drainage of Endorem particles from the tumor in *ex vivo* colorectal tissue is possible by mechanical actuation, such as massage. Other physiological mechanisms of lymphatic transport, including macrophage uptake which is normally present in living tissue [37], are, therefore, not necessary for the selection of SLNs in colorectal cancer. After *ex vivo* injection, the particles flow via the interstitial space through the lymphatics to the SLNs, driven by mechanical pressure induced by massage. In *in vivo* cases SPIO accumulates normally in macrophages, but this activity is believed to cease soon after resection of the specimen. Other studies have shown the utility of *ex vivo* SLNM in colorectal cancer using a noncolloidal blue dye [20]–[25]. This study has shown that despite the use of particles in *ex vivo* SLNM, the tracer ends up in lymph nodes. The use of particles might even be contributing to accurate sentinel node selection, since the chance of selection of second echelon nodes might be reduced. The specific clinical value of the use of magnetic nanoparticles in colorectal SLN mapping should be investigated in a more elaborate patient study.

The accumulated particles in SLNs are detectable by highly sensitive laboratory equipment. Although Endorem was a pragmatic choice for reasons of availability, it performed well as tracer for SLNs. However, further development of magnetic SLNM in colorectal cancer should consider the optimal magnetic and hydrodynamic particle size and composition. The success of technetium based SLN procedures has shown to be dependent on the particle size of the applied colloid [50], [51]. The development of magnetic nanoparticles with a higher (magnetic) yield will lower the requirements for new clinical instruments to be developed or may increase the sensitivity of the procedure.

For several reasons, an experimental laboratory VSM system is not suitable for clinical applications. The large magnetic fields and helium cooling, as well as sample mounting and long measuring time, are significant drawbacks for clinical use of a VSM. Therefore, further development of fast, high-sensitive magnetic detectors is desirable. Exploiting the nonlinear behavior of the SPIO particles in AC susceptometry or a frequency mixing technique [52], the detection can be very specific, which is mandatory for samples with unknown diamagnetic content. In colorectal cancer, the SLNs have to be selected out of a series of about 10–25 resected lymph nodes per patient. Therefore, a clinical magnetic detection instrument with high sensitivity and short processing time would enable pathologists to use their specific microscopy techniques for ultrastaging on magnetically selected SLNs, so as to find high-risk patients who may benefit from adjuvant therapy.

C. Other Techniques of SPIO Quantification

In the literature, several other techniques to quantify SPIO in biological samples are described. Besides magnetometry, optical and mass spectroscopies are used to analyze SPIO content in cell samples. Inductively coupled plasma spectroscopy is a highly sensitive but expensive method that is not suitable for routine sample analysis. These techniques are very sensitive for SPIO, but require sample digestion which is not compatible with histopathologic analysis in SLNM [28], [53], [54].

Since Endorem is developed as MRI contrast agent, the uptake of particles can be revealed by MRI. MRI techniques to quantify SPIO concentrations in samples are based on the field inhomogeneities produced by the particles. These field inhomogeneities can be quantified by measuring a reduction in relaxation time [53] or by model-based reconstruction based on a measured phase map [55], [56]. Boutry and colleagues could quantify magnetic nanoparticle content in cell samples by relaxometry [53], however, their procedure is not applicable in SLNM because it requires sample digestion and thus, impedes histopathologic analysis of intact samples. Problematic in SPIO quantification with MRI are other sources of field

inhomogeneities in a sample, like gradient instabilities and tissue–tissue or air–tissue interfaces that all may cause the contribution from SPIO nanoparticles to be indistinguishable [27], [56]. Therefore, (background) measurements that allow identification of these other components are often required to determine the exact contribution from SPIO [55], [57], [58]. This makes MRI procedures much more complex and time consuming, since in case of SLNM, the SLNs also have to be measured before tracer administration. For *ex vivo* procedures, this would postpone the time-critical tracer injection, and therefore, the identification rate of the procedure may become affected. Finally, MRI is an expensive technique which is less specific for nonlinear magnetic properties and, therefore, less suitable for *ex vivo* SLNM with SPIO. Therefore, magnetometry is more selective for the specific nonlinear characteristics of SPIO can be much more accurate, less expensive, and easier to implement in clinical practice.

IV. Conclusion

SLN mapping using superparamagnetic nanoparticles is successfully applied in colorectal cancer patients. Although a dispersion of nanoparticles is used in the *ex vivo* tissue, the tracer ends up in lymph nodes. This study shows that nondestructive VSM measurements on fresh or formalin-fixated lymph nodes can reveal the magnetic properties inside, provided that the lymph nodes are firmly fastened. The nonlinear superparamagnetic contribution arising from the magnetic nanoparticles in the tracer is distinguishable and quantifiable by modeling the magnetic moment curve with the Langevin model and a bimodal log-normal core size distribution. Furthermore, detection and selection of Endorem-filled SLNs in *ex vivo* colorectal tissue was proven to be possible by a detection limit of 1 μg iron. Selection of the SLN in colorectal cancer using a selective colloidal magnetic tracer can help to accurately intensify standard histopathological analysis by additional staining of those nodes that most probably contain metastases. To facilitate the clinical application of magnetic SLN detection in colorectal cancer, a clinical magnetometer has to be developed that allows quick and specific detection of the nonlinear properties of superparamagnetic tracer in lymph nodes.

References

[1] Q. A. Pankhurst, N. T. K. Thanh, S. K. Jones, and J. Dobson. (2009). Progress in applications of magnetic nanoparticles in biomedicine. *J. Phys. D Appl. Phys.* [Online]. *42(22)*, p. 224001, Available: http://stacks.iop.org/0022-3727/42/i=22/a=224001

[2] S. Laurent, D. Forge, M. Port, A. Roch, C. Robic, L. Vander Elst, and R. N. Muller. (2008). Magnetic iron oxide nanoparticles: Synthesis, stabilization, vectorization, physicochemical characterizations, and biological applications. *Chem. Rev.* [Online]. *108(6)*, pp. 2064–2110, Available: http://pubs.acs.org/doi/abs/10.1021/cr068445e

[3] C. Corot, P. Robert, J.-M. Idée, and M. Port. (2006). Recent advances in iron oxide nanocrystal technology for medical imaging. *Adv. Drug Del. Rev.* [Online]. *58(14)*, pp. 1471–1504, Available: http://dx.doi.org/10.1016/j.addr.2006.09.013

[4] J. W. M. Bulte and D. L. Kraitchman. (2004). Iron oxide MR contrast agents for molecular and cellular imaging. *NMR Biomed.* [Online]. *17(7)*, pp. 484–499, Available: http://dx.doi.org/10.1002/nbm.924

[5] A. Ito, M. Shinkai, H. Honda, and T. Kobayashi. (2005). Medical application of functionalized magnetic nanoparticles. *J. Biosci. Bioeng.* [Online]. *100(1)*, pp. 1–11, Available: http://dx.doi.org/10.1263/jbb.100.1

[6] T. Islam and L. Josephson. (2009). Current state and future applications of active targeting in malignancies using superparamagnetic iron oxide nanoparticles. *Cancer Biomarkers* [Online]. *5(2)*, pp. 99–107, Available: http://iospress.metapress.com/content/xp1q51j863644wk4/

[7] R. Ivkov, S. DeNardo, W. Daum, A. Foreman, R. Goldstein, V. Nemkov, and G. DeNardo. (2005). Application of high amplitude alternating magnetic fields for heat induction of nanoparticles localized in cancer. *Clin. Cancer Res.* [Online]. *11(19 II)*, pp. 7093s–7103s, Available: http://clincancerres.aacrjournals.org/content/11/19/7093s.abstract

[8] T. Jain, J. Richey, M. Strand, D. Leslie-Pelecky, C. Flask, and V. Labhasetwar. (2008). Magnetic nanoparticles with dual functional properties: Drug delivery and magnetic resonance imaging. *Biomaterials* [Online]. *29(29)*, pp. 4012–4021, Available: http://dx.doi.org/10.1016/j.biomaterials.2008.07.004

[9] R. Hergt and S. Dutz. (2007). Magnetic particle hyperthermia-biophysical limitations of a visionary tumour therapy. *J. Magn. Magn. Mater.* [Online]. *311(1 SPEC. ISS.)*, pp. 187–192, cited By (since 1996) 90. Available: http://dx.doi.org/10.1016/j.jmmm.2006.10.1156

[10] T. Nakagawa, Y. Minamiya, Y. Katayose, H. Saito, K. Taguchi, H. Imano, H. Watanabe, K. Enomoto, M. Sageshima, T. Ueda, and J. I. Ogawa. (2003). A novel method for sentinel lymph node mapping using magnetite in patients with non-small cell lung cancer. *J. Thoracic Cardiovasc. Surg.* [Online]. *126(2)*, pp. 563–567. Available: http://dx.doi.org/10.1016/S0022-5223(03)00216-2

[11] Y. Minamiya, M. Ito, Y. Katayose, H. Saito, K. Imai, Y. Sato, and J. I. Ogawa, "Intraoperative sentinel lymph node mapping using a new sterilizable magnetometer in patients with nonsmall cell lung cancer," *Ann. Thoracic Surg.*, vol. 81, no. 1, pp. 327–330, 2006.

[12] T. Joshi, Q. A. Pankhurst, S. Hattersley, A. Brazdeikis, M. Hall-Craggs, E. De Vita, A. Bainbridge, R. Sainsbury, A. Sharma, and M. Douek, "Magnetic nanoparticles for detecting cancer spread," in *Proc. 30th Annu. San Antonio Breast Cancer Symp.*, 2007, vol. 106, p. S129.

[13] L. Johnson, Q. A. Pankhurst, A. Purushotham, A. Brazdeikis, and M. Douek. (2010). Magnetic sentinel lymph node detection for breast cancer. *Cancer Res.* [Online]. *70(24)*, pp. P1–01–23, Available: http://cancerres.aacrjournals.org

[14] M. Shiozawa, A. Lefor, Y. Hozumi, K. Kurihara, N. Sata, Y. Yasuda, and M. Kusakabe. (2012). Sentinel lymph node biopsy in patients with breast cancer using superparamagnetic iron oxide and a magnetometer. *Breast Cancer* [Online]. pp. 1–7. Available: http://dx.doi.org/10.1007/s12282-011-0327-9

[15] S. Tanaka, H. Ota, Y. Kondo, Y. Tamaki, S. Kobayashi, and S. Noguchi. (2003, Jun.). Detection of magnetic nanoparticles in lymph nodes of rat by high T_c-SQUID. *IEEE Trans. Appl. Supercond.* [Online]. *13(2)*, pp. 377–380, Available: http://dx.doi.org/10.1109/TASC.2003.813857.

[16] D. J. Grootendorst, J. Jose, R. M. Fratila, M. Visscher, A. H. Velders, B. Ten Haken, T. G. Van Leeuwen, W. Steenbergen, S. Manohar, and T. J. M. Ruers, "Evaluation of superparamagnetic iron oxide nanoparticles (endorem) as a photoacoustic contrast agent for intra-operative nodal staging," *Contrast Media Molecular Imag.*, vol. 8, no. 1, pp. 83–91, 2013.

[17] A. H. Strickland, N. Beechey-Newman, C. B. Steer, and P. G. Harper. (2002). Sentinel node biopsy: An in depth appraisal. *Crit. Rev. Oncol./Hematol.* [Online]. *44(1)*, pp. 45–70, Available: http://dx.doi.org/10.1016/S1040-8428(02)00018-5

[18] P. J. Tanis, O. E. Nieweg, R. A. Valdés Olmos, and B. B. Kroon. (2001). Anatomy and physiology of lymphatic drainage of the breast from the perspective of sentinel node biopsy. *J. Amer. Coll. Surg.* [Online]. *192(3)*, pp. 399–409, Available: http://dx.doi.org/10.1016/S1072-7515(00)00776-6

[19] E. S. van der Zaag, W. H. Bouma, P. J. Tanis, D. T. Ubbink, W. A. Bemelman, and C. J. Buskens. (2012). Systematic review of sentinel lymph node mapping procedure in colorectal cancer. *Ann. Surg. Oncol.* [Online]. vol. 19, pp. 3449–3459. Available: http://dx.doi.org/10.1245/s10434-012-2417-0

[20] A. Stojadinovic, P. J. Allen, M. Protic, J. F. Potter, C. D. Shriver, J. M. Nelson, and G. E. Peoples. (2005). Colon sentinel lymph node mapping: Practical surgical applications. *J. Amer. Coll. Surg.* [Online]. *201(2)*, pp. 297–313, Available: http://dx.doi.org/10.1016/j.jamcollsurg.2005.01.020

[21] J. Tuech, P. Pessaux, F. D. Fiore, V. Nitu, B. Lefebure, A. Colson, and F. Michot. (2006). Sentinel node mapping in colon carcinoma: In-vivo versus ex-vivo approach. *Eur. J. Surg. Oncol. (EJSO)* [Online]. *32(2)*, pp. 158–161, Available: http://dx.doi.org/10.1016/j.ejso.2005.11.004

[22] E. S. van der Zaag, C. J. Buskens, N. Kooij, H. Akol, H. M. Peters, W. H. Bouma, and W. A. Bemelman. (2009). Improving staging accuracy in colon and rectal cancer by sentinel lymph node mapping: A comparative

study. *Eur. J. Surg. Oncol. (EJSO)* [Online]. *35(10)*, pp. 1065–1070, Available: http://dx.doi.org/10.1016/j.ejso.2009.02.001

[23] P. M. van Schaik, J. C. van der Linden, M. F. Ernst, W. A. H. Gelderman, and K. Bosscha. (2007). Ex vivo sentinel lymph node "mapping" in colorectal cancer. *Eur. J. Surg. Oncol.* [Online]. *33(10)*, pp. 1177–1182, Available: http://dx.doi.org/10.1016/j.ejso.2007.03.006

[24] C. T. Viehl, C. T. Hamel, W. R. Marti, U. Guller, L. Eisner, U. Stammberger, L. Terracciano, H. P. Spichtin, F. Harder, and M. Zuber. (2003). Identification of sentinel lymph nodes in colon cancer depends on the amount of dye injected relative to tumor size. *World J. Surg.* [Online]. vol. 27, pp. 1285–1290. Available: http://dx.doi.org/10.1007/s00268-003-7086-5

[25] J. H. Wong, S. Steineman, C. Calderia, J. Bowles, and T. Namiki. (2001). Ex vivo sentinel node mapping in carcinoma of the colon and rectum. *Ann. Surg.* [Online]. *233(4)*, pp. 515–521, Available: http://www.ncbi.nlm.nih.gov/pmc/articles/PMC1421280/

[26] V. Galimberti, S. Zurrida, M. Intra, S. Monti, P. Arnone, G. Pruneri, and C. De Cicco. (2000). Sentinel node biopsy interpretation: The milan experience. *Breast J.* [Online]. *6(5)*, pp. 306–309, Available: http://dx.doi.org/10.1046/j.1524-4741.2000.20062.x

[27] W. Liu and J. A. Frank, "Detection and quantification of magnetically labeled cells by cellular MRI," *Eur. J. Radiol.*, vol. 70, no. 2, pp. 258–264, 2009.

[28] E. R. Dadashzadeh, M. Hobson, L. Henry Bryant, D. D. Dean, and J. A. Frank, "Rapid spectrophotometric technique for quantifying iron in cells labeled with superparamagnetic iron oxide nanoparticles: Potential translation to the clinic," *Contrast Media Molecular Imag.*, vol. 8, no. 1, pp. 50–56, 2013.

[29] W. Beyhum, D. Hautot, J. Dobson, and Q. A. Pankhurst. (2005). Magnetic biomineralisation in huntington's disease transgenic mice. in *Proc. J. Phys. Conf. Series* [Online]. *17(1)*, p. 50, Available: http://stacks.iop.org/1742-6596/17/i=1/a=008

[30] J. Dobson and P. Grassi. (1996). Magnetic properties of human hippocampal tissue -evaluation of artefact and contamination sources. *Brain Res. Bull.* [Online]. *39(4)*, pp. 255–259, Available: http://dx.doi.org/10.1016/0361-9230(95)02132-9

[31] D. Hautot, Q. A. Pankhurst, and J. Dobson. (2005). Superconducting quantum interference device measurements of dilute magnetic materials in biological samples. *Rev. Sci. Instrum.* [Online]. *76(4)*, p. 045101. Available: http://dx.doi.org/10.1063/1.1868272

[32] D. Hautot, Q. A. Pankhurst, C. M. Morris, A. Curtis, J. Burn, and J. Dobson, "Preliminary observation of elevated levels of nanocrystalline iron oxide in the basal ganglia of neuroferritinopathy patients," *Biochim. Biophys. Acta - Molecular Basis Disease*, vol. 1772, no. 1, pp. 21–25, 2007.

[33] J. L. Kirschvink, A. Kobayashi-Kirschvink, and B. J. Woodford, "Magnetite biomineralization in the human brain," *Proc. Nat. Acad. Sci. United States America*, vol. 89, no. 16, pp. 7683–7687, 1992.

[34] Q. A. Pankhurst, D. Hautot, N. Khan, and J. Dobson, "Increased levels of magnetic iron compounds in Alzheimer's disease," *J. Alzheimer's Disease*, vol. 13, no. 1, pp. 49–52, 2008.

[35] I. Raynal, P. Prigent, S. Peyramaure, A. Najid, C. Rebuzzi, and C. Corot, "Macrophage endocytosis of superparamagnetic iron oxide nanoparticles: Mechanisms and comparison of ferumoxides and ferumoxtran-10," *Investigat. Radiol.*, vol. 39, no. 1, pp. 56–63, 2004.

[36] H. Y. Lee, S. H. Lee, C. Xu, J. Xie, J. H. Lee, B. Wu, A. Leen Koh, X. Wang, R. Sinclair, S. X. Wang, D. G. Nishimura, S. Biswal, S. Sun, S. H. Cho, and X. Chen, "Synthesis and characterization of PVP-coated large core iron oxide nanoparticles as an MRI contrast agent," *Nanotechnology*, vol. 19, no. 16, art. no. 165101, 6 pp., 2008.

[37] M. A. Saksena, A. Saokar, and M. G. Harisinghani, "Lymphotropic nanoparticle enhanced MR imaging (LNMRI) technique for lymph node imaging," *Eur. J. Radiol.*, vol. 58, no. 3, pp. 367–374, 2006.

[38] D. X. Chen, O. Pascu, A. Roig, and A. Sanchez, "Size analysis and magnetic structure of nickel nanoparticles," *J. Magn. Magn. Mater.*, vol. 322, no. 24, pp. 3834–3840, 2010.

[39] C. W. Jung and P. Jacobs. (1995). Physical and chemical properties of superparamagnetic iron oxide MR contrast agents: Ferumoxides, ferumoxtran, ferumoxsil. *Magn. Reson. Imag.* [Online]. *13(5)*, pp. 661–674, Available: http://dx.doi.org/10.1016/0730-725X(95)00024-B

[40] C. P. Bean and I. S. Jacobs. (1956). Magnetic granulometry and superparamagnetism. *J. Appl. Phys.* [Online]. *27(12)*, pp. 1448–1452, Available: http://link.aip.org/link/doi/10.1063/1.1722287

[41] D. X. Chen, A. Sanchez, E. Taboada, A. Roig, N. Sun, and H. C. Gu. (2009). Size determination of superparamagnetic nanoparticles from magnetization curve. *J. Appl. Phys.* [Online]. *105(8)*, p. 083924. Available: http://dx.doi.org/10.1063/1.3117512

[42] C. G. Granqvist and R. A. Buhrman, "Ultrafine metal particles," *J. Appl. Phys.*, vol. 47, no. 5, pp. 2200–2219, 1976.

[43] L. B. Kiss, J. Söderlund, G. A. Niklasson, and C. G. Granqvist. (1999). New approach to the origin of lognormal size distributions of nanoparticles," *Nanotechnology* [Online]. *10(1)*, p. 25, Available: http://stacks.iop.org/0957-4484/10/i=1/a=006

[44] E. V. Groman, L. Josephson, and J. M. Lewis, "Biologically degradable superparamagnetic materials for use in clinical applications," U.S. Patent 4827945, May 9, 1989.

[45] M. Blanco-Mantecón and K. O'Grady, "Grain size and blocking distributions in fine particle iron oxide nanoparticles," *J. Magn. Magn. Mater.*, vol. 203, no. 1–3, pp. 50–53, 1999.

[46] S. Biederer, T. Knopp, T. F. Sattel, K. Lüdtke-Buzug, B. Gleich, J. Weizenecker, J. Borgert, and T. M. Buzug. (2009). Magnetization response spectroscopy of superparamagnetic nanoparticles for magnetic particle imaging. *J. Phys. D Appl. Phys.* [Online]. *42(20)*, p. 205007, Available: http://stacks.iop.org/0022-3727/42/i=20/a=205007

[47] J. C. Lagarias, J. A. Reeds, M. H. Wright, and P. E. Wright. (1998, May). Convergence properties of the Nelder–Mead simplex method in low dimensions. *SIAM J. Optim.* [Online]. *9(1)*, pp. 112–147, Available: http://dx.doi.org/10.1137/S1052623496303470

[48] J. E. Lima, A. L. Brandl, A. D. Arelaro, and G. F. Goya. (2006). Spin disorder and magnetic anisotropy in Fe_3O_4 nanoparticles. *J. Appl. Phys.* [Online]. *99(8)*, p. 083908, Available: http://link.aip.org/link/?JAP/99/083908/1

[49] L. F. Gamarra, G. E. S. Brito, W. M. Pontuschka, J. B. Mamani, C. A. Moreira-Filho, and E. Amaro Jr. (2007). Study of the ferrofluid drying process for morphological and nanostructutal characterization. *Braz. J. Phys.* [Online]. vol. 37, pp. 1288–1291, Available: http://dx.doi.org/10.1590/S0103-97332007000800016

[50] M. R. S. Keshtgar and P. J. Ell, "Sentinel lymph node detection and imaging," *Eur. J. Nuclear Med.*, vol. 26, no. 1, pp. 57–67, 1999.

[51] M. H. Leidenius, E. A. Leppänen, L. A. Krogerus, and K. A. V. Smitten, "The impact of radiopharmaceutical particle size on the visualization and identification of sentinel nodes in breast cancer," *Nuclear Med. Commun.*, vol. 25, no. 3, pp. 233–238, 2004.

[52] H. J. Krause, N. Wolters, Y. Zhang, A. Offenhäusser, P. Miethe, M. H. F. Meyer, M. Hartmann, and M. Keusgen. (2007). Magnetic particle detection by frequency mixing for immunoassay applications. *J. Magn. Magn. Mater.* [Online]. *311(1 SPEC. ISS.)*, pp. 436–444, Available: http://dx.doi.org/10.1016/j.jmmm.2006.10.1164

[53] S. Boutry, D. Forge, C. Burtea, I. Mahieu, O. Murariu, S. Laurent, L. Vander Elst, and R. N. Muller, "How to quantify iron in an aqueous or biological matrix: a technical note," *Contrast Media Molecular Imag.*, vol. 4, no. 6, pp. 299–304, 2009.

[54] P. Danhier, G. De Preter, S. Boutry, I. Mahieu, P. Leveque, J. Magat, V. Haufroid, P. Sonveaux, C. Bouzin, O. Feron, R. N. Muller, B. F. Jordan, and B. Gallez. (2012). Electron paramagnetic resonance as a sensitive tool to assess the iron oxide content in cells for MRI cell labeling studies," *Contrast Media Molecular Imag.* [Online]. *7(3)*, pp. 302–307, Available: http://dx.doi.org/10.1002/cmmi.497

[55] P. Cantillon-Murphy, L. L. Wald, M. Zahn, and E. Adalsteinsson, "Measuring SPIO and Gd contrast agent magnetization using 3T MRI," *NMR Biomed.*, vol. 22, no. 8, pp. 891–897, 2009.

[56] J. Langley, W. Liu, E. K. Jordan, J. A. Frank, and Q. Zhao, "Quantification of SPIO nanoparticles in vivo using the finite perturber method," *Magn. Reson. Med.*, vol. 65, no. 5, pp. 1461–1469, 2011.

[57] R. M. Weisskoff and S. Kiihne, "MRI susceptometry: Image-based measurement of absolute susceptibility of MR contrast agents and human blood," *Magn. Reson. Med.*, vol. 24, no. 2, pp. 375–383, 1992.

[58] P. H. Mills, T. K. Hitchens, L. M. Foley, T. Link, Q. Ye, C. R. Weiss, J. D. Thompson, W. D. Gilson, A. Arepally, J. A. Melick, P. M. Kochanek, C. Ho, J. W. M. Bulte, and E. T. Ahrens, "Automated detection and characterization of SPIO-labeled cells and capsules using magnetic field perturbations," *Magn. Reson. Med.*, vol. 67, no. 1, pp. 278–289, 2012.

Authors' photographs and biographies not available at the time of publication.